Experimental and numerical investigation of fracturing mechanism in concrete by using deflagration agent

Kazuma Moriya[1,a], Daisuke Fukuda[1,b], Katsuhiko Kaneko[2,c], Katsuya Sasaki[3,d] and Ryo Sakamoto[3,e]

[1] Graduate School of Engineering, Hokkaido University, Kita 13 Nishi 8, Kita-ku, Sapporo, Hokkaido 060-8628, Japan

[2] Faculty of Engineering, Hokkaido University, Kita 13 Nishi 8, Kita-ku, Sapporo, Hokkaido 060-8628, Japan

[3] Hitachi Zosen Co., Nankoukita 1-7-89, Sumieno-ku, Osaka 559-8559, Japan

[a] m-kazuma@geo-er.eng.hokudai.ac.jp, [b] daichang@geo-er.eng.hokudai.ac.jp, [c] Kaneko@geo-er.eng.hokudai.ac.jp, [d] sasaki_ka@hitachizosen.co.jp, [e] sakamoto_r@hitachizosen.co.jp

Keywords: Dynamic Fracturing, Deflagration, Finite Element Method, Material Heterogeneity

Abstract. Although a design method for fracturing concrete and rocks using deflagration agents is strongly required, the fracture mechanism due to deflagration has not yet been well understood. We conducted experiment studies and numerical simulations of the fracturing of concrete, and found that the obtained results for both were in good agreement. Furthermore, we numerically investigated the design for an in-situ application. Therefore, the proposed method could be applied to understand the fracture mechanism due to deflagration agents and to achieve a design method for the technique.

Introduction

Understanding the fracture mechanisms of quasi-brittle materials such as concrete and rocks is of considerable importance in various fields of engineering. In particular, in civil and mining engineering, fracture control caused by the application of rapid loads is an important issue because of the frequent use of blasting for operations such as tunnel excavation and excavation in mining. Therefore, in order to achieve safe operation and stable production in mines, it is essential to develop optimal and economical deign methods for fracture control.

Although blasting, in which explosives are detonated to fracture concrete and rocks, is a well-known fracturing technique, its application is occasionally limited by legal regulations regarding the use of explosives and the generation of harmful vibrations and noise effects in the surrounding environment. To avoid such problems, alternative techniques involving the use of deflagration agents have been proposed. The electric discharge impulse crushing method (EDICM) is a fracturing technique that uses both electric discharge and a deflagration agent, i.e. liquid-nitromethane (NM) [1] for fracturing concrete and rocks. However, the design method for this technique has not been established because the fracture mechanisms due to deflagration agents have not yet been well understood.

Typically, fracturing due to rapidly applied loads completes within at most a few to several hundred microseconds. Therefore, experimental investigations of the fracture mechanism are challenging because of the lack of useful experimental methods for the evaluation of fracturing in such a short time scale. Therefore, in this study, we simulate fracturing due to the deflagration of NM through

EDICM using a dynamic fracture process analysis (DFPA) code [2,3,4]. Additionally, in order to develop a design method in EDICM as a case study, we applied DFPA to controlled splitting as an in-situ application of EDICM.

Modelling methodology for deflagration of NM

Because the applied pressure waveform, i.e. loading rate or strain rate, is a quite important factor [3,5] for the characterization of the fracture mechanism, the deflagration phenomenon of NM in EDICM is modelled using DFPA. In EDICM, a cylindrical plastic container filled with liquid NM is prepared. A thin metal wire is attached to the inside of the container. An electric discharge generator is used to control the initiation of deflagration. An electric discharge is produced, and the plasma generated as a result vaporizes the abovementioned wire. With the vaporization, the deflagration of NM commences. Therefore, when the container is set in charge holes drilled into the target material to be split, the gas expansion due to the deflagration causes fracturing in concrete and rocks.

To consider the characteristics of the pressure generated in the charge hole, the pressure was measured using a hollow cylindrical austenite stainless steel chamber, a schematic of which is shown in Fig. 1. The plastic container filled with NM was set inside the steel chamber, and the hollow part was confined by upper and lower flanges. The outside diameter, inside diameter, and length in the axial direction of the hollow were 120, 20, and 70 mm, respectively. The diameter and length of the plastic container were 18 and 70 mm, respectively. The generated pressure was measured using a piezofilm (PVF_2 11-125-EK; Dynasen, Inc.) set at the bottom of the hollow.

In Fig. 2, the dotted line indicates the measured pressure profile. The pressure spike observed immediately after the electric discharge was attributed to both the generation of plasma and the vaporization of the wire [1], and the subsequent gradual increase in pressure was found to be due to the deflagration of NM. The influence of the pressure due to electric discharge on fracturing was found to be negligible because the electric discharge itself only served to initiate deflagration. The peak of the pressure due to the deflagration was achieved around 130 μs after electric discharge.

Considering that the expansion of gaseous products due to the deflagration of NM can be regarded as an isentropic process, we used the Jones-Wilkins-Lee (JWL) equation of state (EOS) [6]. By using the EOS, the volume decoupling ratio [7] can also be considered. Additionally, considering that the detonation velocity of the explosives used in blasting is 3 to 7 km/s and the deflagration velocity of NM is 0.5 km/s, deflagration is a relatively slower phenomenon than detonation. Therefore, in the simulation of deflagration, the EOS of the deflagration gas as well as the deflagration process needs to be considered. Therefore, we assumed the applied pressure, $P(t)$ at time t, due to the deflagration gas to be given by the following equation:

$$P(t) = P_{\mathrm{jwl}}(t) \cdot F_{\mathrm{d}}(t) \tag{1}$$

where $P_{\mathrm{jwl}}(t)$ is the JWL EOS for NM and is given as

$$P_{\mathrm{jwl}}(t) = A\exp\{-R_1 V(t)/V_{\mathrm{effect}}\} + B\exp\{-R_2 V(t)/V_{\mathrm{effect}}\} + C\{V(t)/V_{\mathrm{effect}}\}^{-(\omega+1)} \tag{2}$$

and $F_{\mathrm{d}}(t)$ is the characteristic function which expresses the fraction of the deflagration and is given as

$$F_{\mathrm{d}}(t) = [A\exp\{-R_1(V_0/V_{\mathrm{d}}(t))\} + B\exp\{-R_2(V_0/V_{\mathrm{d}}(t))\} + C(V_0/V_{\mathrm{d}}(t))^{-(\omega+1)}]/P_{\max} \tag{3}$$

where V_{effect} is the effective volume of the NM considering the influence of the combustion of the plastic container and is given by $V_{effect} = kV_{NM}$, V_0 is the initial volume of the charge hole, $V(t)$ is the volume of expanded gaseous products at time t, and $V_d(t)$ is the deflagrated volume of the NM at time t. The JWL parameters for NM are A = 348.504 GPa, B = 9.021 GPa, C = 1.225 GPa, R_1 = 5.38881, R_2 = 1.39179, ω = 0.57, and P_{max} = 5.05 GPa [8]. The time required for the pressure due to deflagration to reach its maximum value, t_{peak}, was found to be 130 μs from Fig. 2. For $V_d(t)$, we used a quadratically increasing function with respect to time t, and we used a monotonically decreasing function in $V_d(t)$ after $t = t_{peak}$ for simplicity.

The numerical model corresponding to one cross section of the steel chamber used for the pressure measurement was assumed. The size of the model was equivalent to that used in the pressure measurement. All outer boundaries of the model were treated as free faces. This dynamic finite element method (FEM) analysis was conducted in 2-D under the plane strain condition. The physical properties of the steel used in the analysis were P-wave velocity = 6000 m/s, S-wave velocity = 3107 m/s, density = 8000 kg/m^3, Young's modulus = 200 GPa, and Poisson's ratio = 0.3. Fracturing did not occur during the analysis.

In Fig. 2, the solid lines indicate $P(t)$ for analysed coefficient values k of 1.08, 1.03, and 0.97. The time at which the pressure spike due to the electric discharge was detected was considered as the time of commencement of deflagration, i.e. t = 0 in the figure. Fig. 2 clearly shows good agreement between the proposed pressure model, $P(t)$ for k = 1.03 and the measured pressure profile. Because EDICM uses a plastic container for the package of the NM, the volume of the plastic parts contributes to the decoupling effect, leading to a reduction in the amplitude of the obtained pressure. Therefore, the analyzed values may be reasonable in the physical sense. For DFPA conducted in the following sections, $P(t)$ described in this section is applied.

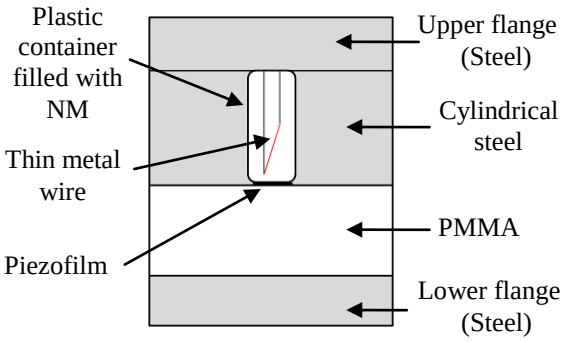

Fig. 1 Schematic of pressure measurement using austenite stainless steel chamber

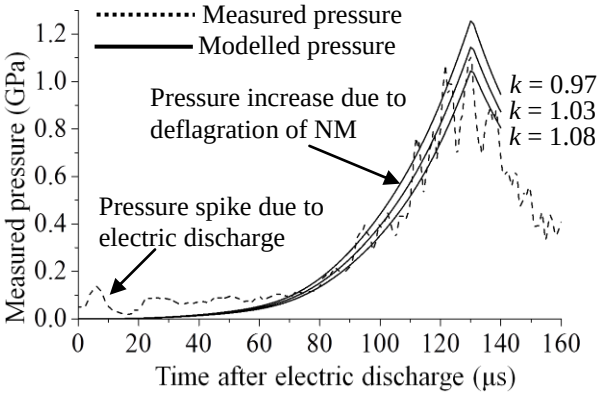

Fig. 2 Measured pressure profile

Numerical simulation method (Dynamic fracture process analysis)

The DFPA [2,3,4] code is based on the 2-D dynamic FEM, and it can simulate crack initiation, propagation, and coalescence mainly in quasi-brittle materials such as concrete and rocks. In addition, fracturing due to tension and compression can be simulated. Finally, DFPA can consider the material heterogeneity and size effect of the strength, which play important roles in the simulation of fracturing in concrete and rocks.

For tensile fracturing, different tensile strengths are assigned to each element boundary such that the strengths satisfy Weibull's distribution [9]. When the computed tensile stress normally acting on the element boundary exceeds the boundary's tensile strength, the fracturing, i.e. crack opening, is expressed by the separation of the element boundary. Non-linear behavior in crack opening is also considered and modelled by using a cohesive law [10] of a bi-linear model [11].

For fracturing due to compression, the shear fracture in materials was judged by the Mohr-Coulomb criteria. After the computed stress state exceeds the Mohr-Coulomb criteria, it is modified to express plastic strain due to fracturing.
All DFPAs were conducted under the plane strain condition in the following section.

Investigation of fracture mechanism in concrete

Fig. 3 shows a photograph of a concrete specimen used in the experiment where the dimensions of the specimen and the alignments of charge holes are also indicated. In this experiment, we assumed controlled splitting along the straight line connecting the charge holes as a representative in-situ application of EDICM. Each charge hole had a diameter and height of 20 and 400 mm, respectively. The plastic container was set at the bottom of the charge holes and the remaining upper space in the holes was tamped by silica sand. It was considered that an electric discharge was applied to the three charge holes simultaneously.
A 2-D finite element mesh corresponding to the concrete specimen was generated, as shown in Fig. 4. The mesh was supposed to include cross sections above the bottom of the charge hole. It contained 146840 elements and 74094 nodal points, respectively, before fracturing. The element sizes in the mesh were carefully chosen to be small enough to minimize the mesh dependency of the crack path. Table 1 lists the physical properties of the concrete used for DFPA. The coefficient of uniformity was set to be sufficiently small enough to express the heterogeneity of concrete. Here, because the heterogeneity of concrete could be one of the important factors affecting the fracture patterns, we conducted three numerical experiments to evaluate the influence by using different spatial strength distributions.
With regard to the boundary conditions, all perimeter boundaries of the mesh were treated as free boundaries. $P(t)$ in Eq. (1) was applied to all the charge holes. With regard to the initiation time lags between charge holes, simultaneous initiation was assumed in all DFPAs.

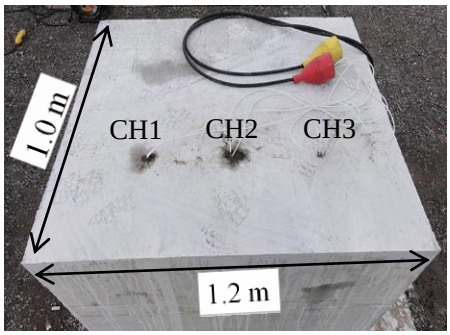

Fig. 3 Concrete block used for experiment

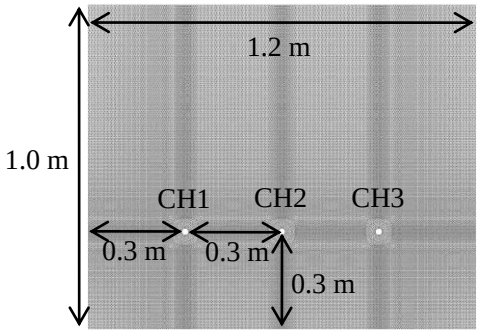

Fig. 4 2-D finitite element mesh used in DFPA

Table 1. Physical properties of concrete used for DFPA

Density (kg/m^3)	2200
P-wave velocity (m/s)	4000
S-wave velocity (m/s)	2450
Young's modulus (GPa)	36.7
Poisson's ratio	0.2

Fracture energy (Pa·m)	75
Mean tensile strength (MPa)	3
Mean compressive strength (MPa)	45
Coefficient of uniformity	5

Results. Fig. 5 shows a photograph of the fractured concrete specimen after the application of EDICM and the fracture planes estimated by DFPA for each strength distribution. In these figures, the white dotted lines indicate predominant opened cracks. A comparison of the experimental and

DFPA results showed good agreement, suggesting that DFPA could successfully express the geometries of the final fracture surface.

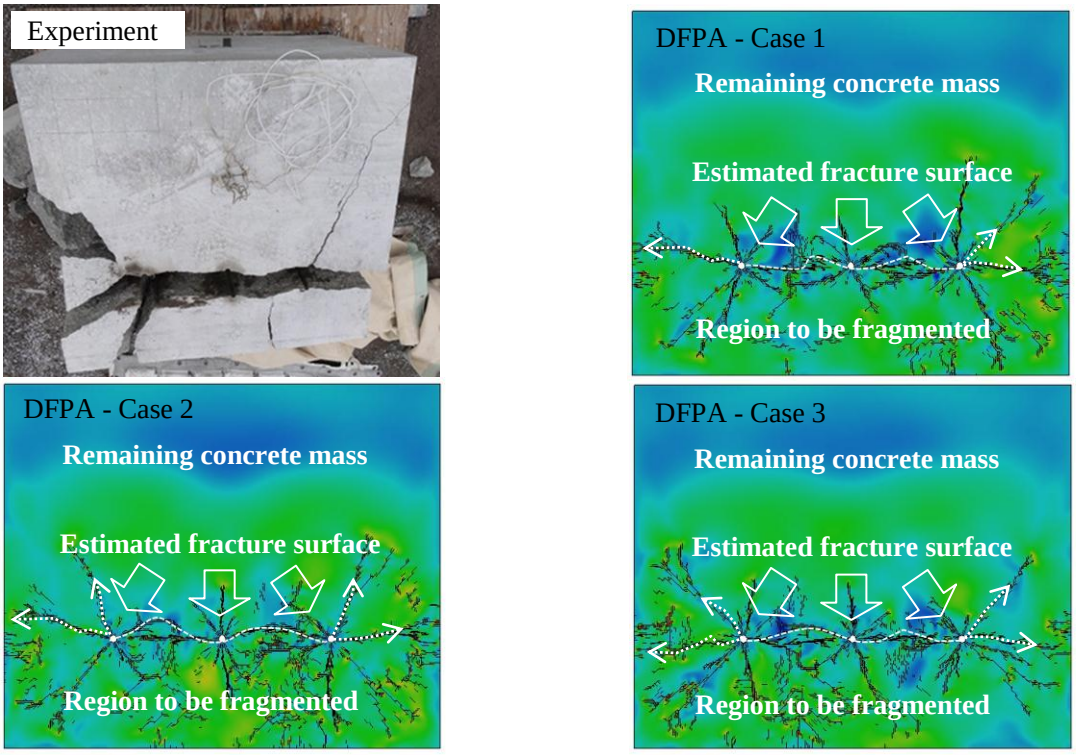

Fig. 5 Comparison of fracture surfaces obtained from experiment and DFPA

In addition, we investigated the fracture mechanism due to deflagration in concrete. Fig. 6 shows the maximum principal stress distribution and crack propagation. The cold and warm colors show compression and tension stresses, respectively. The moving black lines with elapsed time indicate cracks. Time t = 0 in DFPA corresponds to the commencement of the deflagration of NM. Immediately after the application of $P(t)$, the stress waves propagated outward from the charge holes with their initial maximum and minimum principle stresses being in the circumferential and radial directions, respectively. The circumferential and radial stresses were in tension and compression, respectively, before crack initiation. Because of the circumferential stress being in tension, we observed that cracks initiated at approximately t = 40 μs around the charge holes and propagated radially outward from each hole.

With time, some of these cracks became predominant cracks and extended toward the outer free faces while still being cohesive cracks. At t = 80 μs, the number of predominant cracks reduced to 4 through 6. At t = 100 μs, four compressive stress zones (CSZs) were found immediately above and below the middle regions between each charge hole where the stress states were in biaxial compression. The CSZs were found to inhibit the propagation of some of the predominant cracks toward themselves, and little crack extensions were observed around the regions between charge holes. Therefore, after CSZ formation, the predominant cracks from CH1 and CH3 could extend toward the outer boundaries only by avoiding the CSZs. Although the pressure decay commenced after t_{peak} = 130 μs, crack extension continued and the cracks coalesced between the charge holes at t = 160 μs. Following coalescence, i.e. the formation of the final fracture plane between the charge holes, little crack initiations were observed in the region between charge holes, and only the extensions of predominant cracks from CH1 and CH3 were found toward the perimeter boundaries.

Finally, at t = 240 through 260 μs, these predominant cracks reached the left and right outer surfaces, respectively. We assumed that the geometry of the final fracture surface could be estimated from the crack patterns around these time intervals, and we stopped the simulation. The predominant opened cracks at t = 260 μs are indicated by white dotted lines. Considering that the gas generated by deflagration could selectively flow into the opened cracks, as discussed by Kaneko et al. and Cho [4,12], it is reasonable to assume that the predominant opened cracks propagated from the charge holes could continue to extend, which would form the final fracture surface. From this estimation, the parts above and below the estimated fracture surface could remain as a concrete mass and be fragmented into several pieces because of the gas flow, respectively. Note that cracks other than the predominant opened cracks indicated by the white dotted lines are cohesive cracks, i.e. micro-cracks, and therefore, the cohesive cracks simulated by DFPA should be considered as microscopic damage.

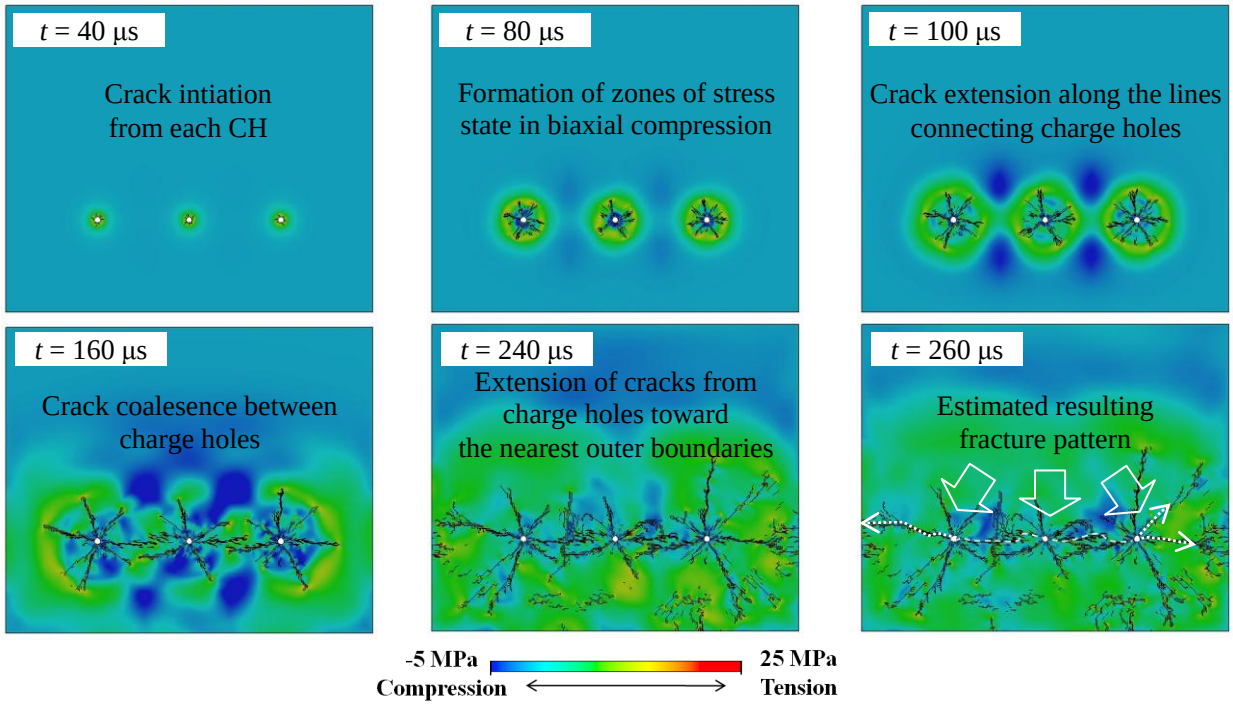

Fig. 6 Fracturing obtained by DFPA for chosen time steps

Discussion. Based on the good agreement between the experimentally and numerically obtained fracture patterns, we consider that the above-mentioned fracture process could help in understanding the fracture mechanism of concrete due to the deflagration of NM.

It is clearly observed that even in the same model geometry, different fracture patterns were obtained depending on the strength distribution. This could be due to the fact that the positions of crack initiation and their propagation direction depend on the strength heterogeneity around each charge hole. On the other hand, for the fracture surface along the charge holes, flatter fracture surfaces were found to be formed with minor differences in their roughness even for different strength distributions. Based on the fracture mechanism obtained from DFPA, it is expected that the crack propagation directions were controlled by CSZ formation. Note that the cracks were found to propagate from each charge hole toward the estimated remaining concrete mass. However, these cracks were still cohesive, and therefore, there were microscopic damages in the remaining concrete. This suggests that the heterogeneity of concrete and the time required for CSZ formation depends on the alignment of charge holes, and that these are important factors for controlled splitting when utilizing deflagration agents.

Numerical design optimization for EDICM

We applied DFPA to the design of controlled splitting for EDICM as a case study. In particular, DFPA was applied to several alignments of charge holes, i.e. spacing and burden, considering the heterogeneity of concrete. Fig. 7 shows an example of the mesh for DFPA. The meshes were supposed to include cross sections above the bottom of the charge hole. In Fig. 7, S and W indicate the spacing and burden, respectively. In this study, spacings of S = 300, 400, 500, and 600 were assumed, with corresponding burdens of W = 0.5S, 0.75S, S, 1.25S, and 1.5S. The physical properties of concrete as listed in Table 1 were also used for DFPA. Here, to evaluate the influence of the heterogeneity of concrete on the fracture patterns, we conducted ten numerical experiments using different strength distributions.

With regard to the boundary conditions, the left, right, and upper perimeter boundaries were treated as continuous boundaries and the lower perimeter boundary was treated as a free face. $P(t)$ in Eq. (1) applied to all CHs and simultaneous initiation was assumed in all DFPAs.

Results & Discussion. Fig. 8 shows the evaluation method for the roughness of the fracture surface. We defined the area between the expected fracture plane and the estimated fracture surface obtained from DFPA divided by the spacing as the roughness of the fracture surface. 20 roughness values were calculated for each charge hole alignment because two fracture surfaces, Region1 and Region2 as shown in Fig. 8, were obtained in each numerical experiment.

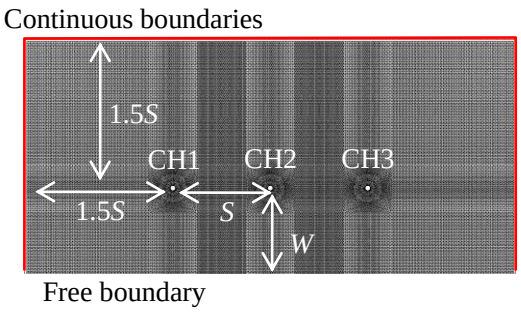

Fig. 7 2-D finitite element mesh used in DFPA

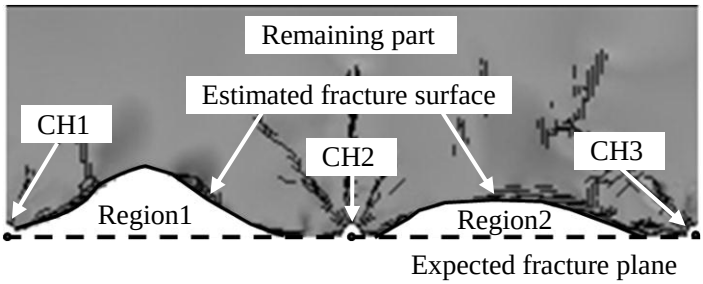

Fig. 8 Definition of roughness

The obtained roughness values and standard deviations of 20 cases for each spacing and burden condition are listed in Table 2. For the same spacing condition, the roughness is similar irrespective of the burden condition. This could be attributed to the CSZs found immediately above and below the middle regions between each charge hole being formed simultaneously because of the same spacing condition. For different spacing conditions, the averaged roughness of fracture surfaces between charge holes was clearly observed to increase with the spacing. This is attributable to CSZ formation being delayed for large spacing conditions. In addition, the standard deviations of the roughness were found to increase with large spacing conditions. These results suggest that the positions of crack initiation and their propagation direction depending on the heterogeneity of the strength around each charge hole dominantly influence the fracture patterns because of the delay in CSZ formation. Based on the above results and discussion, with regard to controlled splitting along charge holes due to deflagration, flatter fracture surfaces could be achieved to determine the optimal spacing where the crack propagation directions are controlled by CSZ formation irrespective of the heterogeneity of concrete.

Table 3. Roughness of fracture surface obtained by DFPA

Spacing (mm)	**Roughness of fracture surface ± standard deviations (mm)**				
	Burden/Spacing				
	0.5	0.75	1.0	1.25	1.5
300	19.15 ± 12.20	19.50 ± 10.70	20.10 ± 13.80	18.15 ± 10.35	22.90 ± 10.33
400	33.66 ± 14.65	35.93 ± 16.48	37.25 ± 15.56	33.76 ± 13.14	39.04 ± 12.89
500	64.45 ± 22.34	58.16 ± 23.01	61.99 ± 25.66	56.99 ± 21.63	61.84 ± 23.78
600	88.93 ± 42.52	81.56 ± 39.46	84.19 ± 38.86	83.75 ± 45.19	88.57 ± 42.18

Concluding remarks

We investigated the fracture mechanism in concrete due to the deflagration of NM through EDICM, a splitting method for concrete and rocks. For this purpose, we used DFPA code based on 2-D FEM. By incorporating a new pressure modelling method based on pressure measurement into DFPA, we could obtain fracture patterns in concrete that were similar to those obtained experimentally for controlled splitting along charge holes.

Based on the success of DFPA, we discussed the detailed fracture process due to the deflagration of NM and investigated the influence of the alignment of charge holes on the roughness of fracture surfaces as a case study of a design method for EDICM. CSZ formation was found above and below the middle regions between charge holes. The utilization of these CSZs was found to be a quite important factor if the flatness of the fracture surface was the main purpose of the controlled splitting of concrete. It was also found that smaller spacings are required between charge holes for the successful utilization of the CSZs because the time required for CSZ formation could increase with the spacing.

References

[1] K. Sasaki, H. Kitajima, H. Maehata, R. Sakamoto and S. Kubota: Proc. 37th Annual Conference on Explosives & Blasting Thechnique, (2011), p. 301-311

[2] K. Kaneko, Y. Matsunaga and M. Yamamoto: Kayaku Gakkaishi, Vol. 56 (1995), p. 207-215 (In Japanese)

[3] S.H. Cho and K. Kaneko: Int J Rock Mech Min Sci, Vol. 41 (2004), p. 771-784

[4] S.H. Cho: Dynamic fracture process analysis of rock and its application to fragmentation control in blasting, PhD thesis, Hokkaido University, Sapporo (2003)

[5] Z.X. Zhanga, S.Q. Koub, J. Yua, Y. Yua, L.G. Jianga and P.-A. Lindqvistb: Int J Rock Mech Sci, Vol. 36 (1999), p. 596-611

[6] E. Lee, M. Finger and W. Collins: JWL Equation of State Coefficients for High Explosives, Lawrence Livermore Laboratory, Rept-UCID-16189, (1973)

[7] A. Rustan: *Rock Blasting Terms and Symbols*: *A Dictionary of Symbols and Terms in Rock Blasting and Related Areas like Drilling, Mining and Rock Mechanics*, Taylor & Francis, (1998), p. 40-155

[8] K. Tanaka: Detonation Properties of High Explosives Calculated by Revised Hihara-Hikita Equation of State, Proc. Eighth Symposium (International) on Detonation, (1985), p. 548-557

[9] W. Weibull: J Appl Mech, Vol. 18 (1951), p. 293-297

[10] A. Hillerborg, M. Modder and P.E. Peterson: Cem Conc, Vol. 6 (1973), p. 773-782

[11] P.E. Peterson: Crack Growth and Development of Fracture Zones in Plain Concrete and Similar Materials, Lund Institute of Technology, Report TVBM-1006 (1981)

[12] K. Kaneko and S.H. Cho: Jpn J Multiph Flow, Vol. 16 (2002), p. 346-352 (In Japanese with English abstract)